Journal of
Plankton Research

plankt.oxfordjournals.org

J. Plankton Res. (2016) 38(2): 183–198. First published online September 30, 2015 doi:10.1093/plankt/fbv086

Costa Rica Dome: Flux and Zinc Experiments

Patterns of microbial community biomass, composition and HPLC diagnostic pigments in the Costa Rica upwelling dome

ANDREW G. TAYLOR[1], MICHAEL R. LANDRY[1]*, ALEXANDRA FREIBOTT[1], KAREN E. SELPH[2] AND ANDRÉS GUTIÉRREZ-RODRÍGUEZ[3]

[1]SCRIPPS INSTITUTION OF OCEANOGRAPHY, 9500 GILMAN DR., LA JOLLA, CA 92093-0227, USA, [2]DEPARTMENT OF OCEANOGRAPHY, UNIVERSITY OF HAWAII AT MANOA, HONOLULU, HI 96822, USA AND [3]STATION BIOLOGIQUE DE ROSCOFF, PLACE GEORGES TEISSIER, 29682 ROSSCOFF CREDEX, FRANCE

*CORRESPONDING AUTHOR: mlandry@ucsd.edu

Received May 17, 2015; accepted September 10, 2015

Corresponding editor: Pia Moisander

We investigated biomass, size-structure, composition, depth distributions and spatial variability of the phytoplankton community in the Costa Rica Dome (CRD) in June–July 2010. Euphotic zone profiles were sampled daily during Lagrangian experiments in and out of the dome region, and the community was analyzed using a combination of digital epifluorescence microscopy, flow cytometry and HPLC pigments. The mean depth-integrated biomass of phytoplankton ranged 2-fold, from 1089 to 1858 mg C m^{-2} (mean ± SE = 1378 ± 112 mg C m^{-2}), among 4 water parcels tracked for 4 days. Corresponding mean (± SE) integrated values for total chlorophyll *a* (Chl *a*) and the ratio of autotrophic carbon to Chl *a* were 24.1 ± 1.5 mg Chl *a* m^{-2} and 57.5 ± 3.4, respectively. Absolute and relative contributions of picophytoplankton (~60%), *Synechococcus* (>33%) and *Prochlorococcus* (17%) to phytoplankton community biomass were highest in the central dome region, while >20 μm phytoplankton accounted for ≤10%, and diatoms <2%, of biomass in all areas. Nonetheless, autotrophic flagellates, dominated by dinoflagellates, exceeded biomass contributions of *Synechococcus* at all locations. Order-of-magnitude discrepancies in the relative contributions of diatoms (overestimated) and dinoflagellates (underestimated) based on diagnostic pigments relative to microscopy highlight potential significant biases associated with making community inferences from pigments.

KEYWORDS: microbial community; biomass; epifluorescence microscopy; flow cytometry; HPLC pigments

available online at www.plankt.oxfordjournals.org

INTRODUCTION

The Costa Rica Dome (CRD) is a wind-driven open-ocean upwelling system associated with the seasonal shoaling of the 10°N thermocline ridge near 9°N and 90°W off the western coast of Central America (Wyrtki, 1964; Fiedler *et al.*, 1991; Fiedler, 2002). The region is known for high abundances of the photosynthetic bacterium *Synechococcus* spp. (up to 3 million cells mL^{-1}), the highest measured in the open ocean (Li *et al.*, 1983; Saito *et al.*, 2005). Such observations underlie the CRD's reputation as a unique and enigmatic upwelling system that is dominated by picophytoplankton but supports high concentrations of zooplankton (Blackburn *et al.*, 1970; Sameoto, 1986; Fiedler, 2002) and flourishing assemblages of higher-order consumers, like tuna, turtles, blue whales and seabirds (Reilly and Thayer, 1990; Vecchione, 1999; McClain *et al.*, 2002; Ballance *et al.*, 2006; Vilchis *et al.*, 2006).

Previous studies in the CRD have analyzed primary producers mainly as chlorophyll *a* (Chl *a*) and flow cytometry populations (Li *et al.*, 1983; Saito *et al.*, 2005; Ahlgren *et al.*, 2014), with very limited microscopy (Franck *et al.*, 2003). To our knowledge, a full community assessment of phytoplankton standing stocks has never been done for the region. This stands in sharp contrast to the eastern equatorial Pacific, another upwelling area which has been well studied by modern techniques in US and French JGOFS (Joint Global Ocean Flux Studies) efforts in the 1990s (Bidigare and Ondrusek, 1996; Chavez *et al.*, 1996; Brown *et al.*, 2003), in subsequent Equatorial Biocomplexity (EB) research in 2004–2005 (Selph *et al.*, 2011; Taylor *et al.*, 2011), and also in experimental studies of perturbation responses to iron fertilization (Landry *et al.*, 2000; Landry and Kirchman, 2002). We know from these studies that the CRD differs markedly from equatorial waters, as well as low-nutrient areas of the central Pacific, in the picophytoplankton dominance of *Synechococcus* (SYN), as opposed to *Prochlorococcus* (PRO), spp., which presumably relates to the different nutrient or trace elemental limitations of these systems (Franck *et al.*, 2003; Saito *et al.*, 2005; Ahlgren *et al.*, 2014). However, the full extent of phytoplankton structural differences or similarities between the CRD and other systems, as well as their implications for ecosystem functioning and dynamics, has heretofore been unexplored.

The CRD Flux and Zinc Experiments cruise in summer 2010 presented an unprecedented opportunity to sample and study the region's phytoplankton assemblages within the context of integrated experimental studies of plankton dynamics and carbon-based fluxes. Here, we report the first determinations of phytoplankton community biomass, size structure, composition, depth distributions and spatial variability derived from combined complementary analyses by epifluorescence microscopy, flow cytometry and high-pressure liquid chromatography (HPLC) pigments. In addition to providing core data for subsequent analyses of the process rates and relationships in this issue (Landry *et al.*, 2016a) and the basis for structural comparisons to other ecosystems, this study provides broader insights into the biases that can arise from pigment-based inferences of phytoplankton composition.

METHODS

Sampling

Samples were collected during the CRD FLUx and Zinc Experiments (FLUZiE) cruise aboard the R/V Melville from 22 June through 25 July 2010 (Landry *et al.*, 2016a). During the cruise, we conducted Lagrangian-like process studies (termed *cycles*) following a satellite-tracked surface drifter for 4 days. The drifter had a holey sock drogue centered at 15 m to stay with water from the upper mixed layer, and a line extending below the drifter used to attach net bags containing bottle experiments, which were incubated for 24 h under *in situ* conditions of temperature and light at 8 depths in the euphotic zone (Landry *et al.*, 2009; Selph *et al.*, 2016). The present results are depth profiles of samples taken directly from CTD Niskin bottles at the start of each experiment during early morning hydrocasts (02:00 local time). They therefore represent the ambient state of the phytoplankton community (biomass, composition and depth distribution) as assessed by three complementary approaches—epifluorescence microscopy, flow cytometry and pigment analyses by HPLC.

Microscopical assessments of nano- and microplankton

Seawater samples of 500 mL were collected for analysis of protistan eukaryotes using digital epifluorescence microscopy. The samples were preserved according to a modified protocol of Sherr and Sherr (Sherr and Sherr, 1993) with 260 μL of alkaline Lugol's solution, immediately followed by 10 mL of buffered formalin and 500 μL of sodium thiosulfate, with gentle mixing between each addition. The fixed samples were stored in the dark at room temperature for 1 h, then stained with 1 mL of proflavin (0.33% w/v) for an additional hour to highlight protein and cell boundaries. Immediately prior to filtration, 1 mL of 4′,6-diamidino-2-phenylindole (DAPI) (0.01 mg mL^{-1}, final concentration) was added to stain cell nuclei. Sample aliquots of 50 mL (small volume, SV)

were filtered onto 25 mm black polycarbonate filters with a 0.8 μm pore size for analysis of small cells (<20 μm cell diameter). The remaining 450 mL volume (large volume, LV) was filtered onto a 25 mm black polycarbonate filter with 8.0 μm pore size for enumeration of large cells (>20 μm). Nylon backing filters (10 μm pore size) were placed under the polycarbonate filters for even cell distribution during filtration, and all filtering was done under gentle vacuum (<100 mmHg). Each filter was then mounted onto a glass slide using immersion oil and a No. 2 cover slip.

Slides were digitally imaged at sea using a Zeiss Axiovert 200 M inverted compound microscope equipped for high-throughput epifluorescence microscopy (EPI) with a motorized focus drive, stage, objective and filters. Digital images were acquired with a Zeiss AxioCam MRc black and white 8-bit CCD camera. All microscope functions were controlled by Zeiss Axiovision software, and images were collected using automated image acquisition. Exposure times for each image were automatically determined by the Axiovision software to avoid over-exposure. SV samples were viewed at 630× magnification, and LV samples were viewed at 200× magnification. A minimum of 20 random positions were imaged for each slide, with each position consisting of three to four fluorescent channels: Chl *a*, DAPI, FITC (SV and LV samples) and phycoerythrin (SV samples only). DAPI is used to visualize DNA in cells, while FITC is used to see the green fluorescence from proflavin (which stains proteins, and therefore cell outlines). Phycoerythrin (PE) is used to see the fluorescence from *Synechococcus* or other PE-bearing cells (cryptophytes). In addition, 5–10 *z*-plane images were acquired at each position and for each fluorescence channel. The resulting *z*-stack images were subsequently combined using an extended depth of field algorithm to produce entirely in-focus images for each position and channel (Chl *a*, DAPI and FITC, PE). These were then false colored (Chl *a* = red, DAPI = blue, FITC = green, PE = orange) and combined to form a single composite 24-bit RGB image for each position.

The combined images were processed and analyzed using ImagePro software to semi-automate the enumeration of eukaryotic cells larger than 1.5 μm in length (Taylor *et al.*, 2014). Whenever possible, 20 positions and >300 cells were counted for each slide. Poor-quality images were discarded. Cells were automatically segmented from the background and outlined. User interaction was then required to check each image, split connected cells, outline cells that did not auto-segment from the background, and delete artifacts and detritus that the software had incorrectly outlined.

Each cell was manually identified and grouped into seven plankton functional groups: diatoms, autotrophic dinoflagellates (A-Dino), prymnesiophytes (Prym), cryptophytes (Crypto), autotrophic flagellates (A-Flag), heterotrophic dinoflagellates (H-Dino) and heterotrophic flagellates (H-Flag). The A- and H-Flag categories contained all cells that could not be clearly placed into the taxon-defined functional groups, which makes the biomass estimates for the taxon-defined groups conservative (i.e. some dinoflagellates and prymnesiophytes with ambiguous characteristics were likely included in the flagellate groups). Autotrophic cells were identified by the presence of Chl *a* (red autofluorescence under blue light excitation), generally clearly packaged in defined chloroplasts. Obvious heterotrophic cells with recently consumed prey were manually excluded from the autotrophs.

Cells were also grouped into three size categories (Pico, <2 μm; Nano, 2–20 μm; Micro, 20–200 μm) based on the lengths of their longest axis. Microscopical size analysis alone defines the composition of Nano and Micro categories. However, the size class for autotrophic picophytoplankton (A-Pico) also includes contributions from the photosynthetic bacteria, *Prochlorococcus* (PRO) and *Synechococcus* (SYN), and <1.5 μm picoautotrophic eukaryotes (P-Euk) enumerated by flow cytometry (described below), in addition to the autotrophic eukaryotic cells between 1.5 and 2.0 μm measured by EPI.

For all size categories, biovolumes (BV; μm^3) were calculated from the length (L) and width (W) measurements of each cell using the geometric formula of a prolate sphere ($BV = 0.524 \times LWH$), assuming $H = W$. Biomass was calculated as carbon (C; pg $cell^{-1}$) using the following equations: $C = 0.288\ BV^{0.811}$ for diatoms and $C = 0.216\ BV^{0.939}$ for non-diatoms (Menden-Deuer and Lessard, 2000).

Picoplankton analysis by flow cytometry

Samples (1 mL) for flow cytometry (FCM) analysis of phototrophic bacteria, *Prochlorococcus* (PRO) and *Synechococcus* (SYN), heterotrophic bacteria (H-Bact) and picoeukaryotes (P-Euk) were preserved with 0.5% paraformaldehyde (final concentration) and flash frozen in liquid nitrogen. On shore, the samples were stored at −80°C, then thawed in batches and stained with Hoechst 34 442 (1 μg mL^{-1}, final concentration) immediately prior to analysis (Campbell and Vaulot, 1993; Monger and Landry, 1993). The analyses were conducted at the SOEST Flow Cytometry Facility (www.soest.hawaii.edu/sfcf) using a Beckman–Coulter Altra flow cytometer equipped with a Harvard Apparatus syringe pump for quantitative analyses and two argon ion lasers tuned to UV (200 mW) and 488 nm (1 W) excitation. Fluorescence signals were collected using filters for Hoechst-bound DNA, phycoerythrin and chlorophyll, normalized to external standards of 0.5-μm

yellow–green (YG) and UV polystyrene beads (Polysciences Inc., Warrington, PA, USA). Listmode data files (FCS 2.0 format) of cell fluorescence and light-scatter properties were acquired with Expo32 software (Beckman–Coulter), and populations were subsequently delineated with FlowJo software (Tree Star, Inc., www.flowjo.com) to define populations based on DNA signal (all cells), absence of photosynthetic pigments (H-Bact), presence of Chl *a* (P-Euk, PRO and SYN), presence of phycoerythrin (SYN) and forward angle light scatter (FALS; relative size).

FCM abundance estimates for PRO and SYN were converted to carbon biomass using carbon per cell conversions estimated for each taxonomic group with a depth-correction based on bead-normalized FALS (Linacre *et al.*, 2010, 2012). Estimates of cell carbon contents for surface samples were made using mean open-ocean, mixed-layer estimates of 32 and 101 fg C cell^{-1} for PRO and SYN, respectively (Garrison *et al.*, 2000; Brown *et al.*, 2008). Then, using the scaling factor FALS$^{0.55}$ as a relative measure of cell biovolume (Binder *et al.*, 1996; Landry *et al.*, 2003), the carbon:cell contents of subsurface populations were determined for each category from the mean cell carbon values in the mixed layer ($FALS_{mean}$) and the FALS ratios $(FALS_{sample}:FALS_{mean})^{0.55}$ for deeper samples.

Cell counts from both microscopy and flow cytometry were used to assess abundances of picoeukaryotic phytoplankton (P-Euk) in two size classes, 1.5–2 and <1.5 μm. The former were determined directly from microscopical counts. The latter were determined by difference between the total small eukaryotic cells counted by flow cytometry and the total microscopy count of <5 μm cells. Assuming that the cell diameters of <1.5 μm P-Euk were in the range of 0.8 and 1.5 μm, a mean biomass estimate of 192 fg C cell^{-1} was computed for the cells in this size category (Menden-Deuer and Lessard, 2000). These were then combined with >1.5 μm P-Euk biomass measured by microscopy to get total P-Euk carbon estimates. Total A-Pico biomass is the sum of SYN and PRO carbon measured from FCM and total carbon of P-Euk.

Taxon-specific pigments from HPLC analysis

Concentrations of lipophilic pigments, chlorophylls and carotenoids were determined by HPLC. For HPLC analysis, 2.2-L samples of seawater were filtered onto Whatman GF/F filters, stored in liquid nitrogen and later extracted in acetone as described by Goericke (Goericke, 2002). An internal standard (canthaxanthin) was added to the samples, which were analyzed on an Agilent 1100 series HPLC system (Agilent Technologies) with a Waters Symmetry C8 column (3.5 μm particle size, 4.6 × 150 mm, silica, reverse-phase). Pigments were eluted using a gradient method with two solvents: (A) a mixture of methanol, acetonitrile and an aqueous pyridine solution (0.25 M, pH = 5) (50:25:25 v:v:v); and (B) a mixture of methanol, acetonitrile and acetone (20:60:20 v:v:v), according to following times and proportions (time, %A, %B): (0, 100, 0), (12, 60, 40), (36, 0, 100), (38, 0, 100), (40, 100, 0). Pigment concentrations were determined for monovinyl chlorophyll *a* (MVChl *a*), divinyl chlorophyll *a* (DVChl *a*), fucoxanthin (FUCO), 19′-butanoyloxyfucoxanthin (BUT), 19′-hexanoyloxyfucoxanthin (HEX), peridinin (PER), prasinoxanthin (PRAS) and zeaxanthin (ZEAX), as well as a variety of other pigments that were either measured in low concentrations or not used here as pigment indicators of specific taxa.

Each major taxa was evaluated for its contribution to TChl *a* (MVChl *a* + DVChl *a*), as described previously (Goericke and Montoya, 1998; Goericke, 2002). Minimization of least squares between measured and calculated TChl *a* resulted in the following pigment ratios (pigment/pigment) for the various taxa: K(MVChl *a*/FUCO) = 1.43 for diatoms; K(MVChl *a*/HEX) = 1.27 and K(FUCO/HEX) = 0.097 for prymnesiophytes; K(MVChl *a*/BUT) = 1.21 and K(HEX/BUT) = 0.22 for pelagophytes; K(MVChl *a*/ZEAX) = 2.1 for *Synechococcus*; K(ZEAX/DVChl *a*) = 1.08 for *Prochlorococcus*; K(MVChl *a*/NEOX) = 7.31 for chlorophytes; and K(MVChl *a*/ALLO) = 5.03 for cryptophytes.

Nutrient analysis

Samples from each depth were analyzed for nitrate, nitrite, ammonium, phosphate and silicate concentration by flow injection analysis at the nutrient laboratory of the University of California, Santa Barbara on a Lachat Instruments QuikChem 8000 using standard wet-chemistry methods (Gordon *et al.*, 1992).

Statistical analyses

Multiple comparison testing for differences in mean parameters between cycles was done using the non-parametric Kruskal–Wallis analysis of variance by ranks test, accounting for tied ranks, using critical values of the *H*-statistic (Zar, 1984). When significant differences ($P = 0.05$) were found between cycle means (i.e. the null hypothesis was rejected), a Dunn multiple comparison test was performed on all relevant pairs, since there were unequal sample sizes between the cycles, using critical values of the *Q*-statistic ($P = 0.05$ or $P = 0.10$). The software program Prism 6.0 (GraphPad Software, Inc.) was used to do these calculations.

RESULTS

Environmental conditions of the study area

Table I gives the dates, locations and sampling depth ranges for the five experimental cycles conducted on the cruise, and the relative positions of the cycles and daily sampling points are shown in Fig. 1. Site selection and physical features are described in detail by Landry *et al.* (Landry *et al.*, 2016a). Cycle 1 was conducted in southward flowing waters relatively close to the Costa Rica coast. After that experiment, a transect survey was run from 6.6°N, 88.5°W to 10°N, 92°W to locate the central dome area, which was the site selected for Cycle 2 at ~9°N, 91°W (Table I). At the end of Cycle 2, we deployed a satellite-tracked surface drifter with a mixed-layer drogue, which was relocated later as the starting location for Cycle 4. Meanwhile, Cycle 3 was conducted in waters northwest of the dome. Finally, Cycle 5 was conducted east of the dome region in waters, believed to be North Equatorial Counter Current (NECC), flowing rapidly toward the coast. By design, as well as by later hydrographic analysis, several connections can be made among the experiments. Cycles 2 and 4 were clearly in the central dome region, and Cycle 1 clearly outside (coastal). Cycle 3 had characteristics of being on the dome periphery. Cycle 5 was located out of the dome region, but has T–S properties most closely resembling Cycle 4 (Landry *et al.*, 2016a).

Hydrocast profiles for all cycles showed strong stratification of temperature, oxygen and nutrients (Fig. 2). Temperature decreased by 10°C or more in the upper 50 m, while oxygen declined by almost an order of magnitude and nitrate increased by 25 μM over the same depth range. The differences among cycles were mainly in depth of the strongest gradients. Profiles from the central dome region (Cycles 2 and 4) had the shallowest mixed layers (19 and 21 m, respectively) and depths of the 20°C isotherm (26 and 32 m, respectively). By Fiedler's criterion for stations in the CRD, the 20°C isotherm ≤35-m depth (Fiedler, 2002), samplings for Cycles 2–4 were conducted in the dome area, and Cycles 1 and 5 were sampled out of the dome. These designations are also reflected in environmental differences of the upper euphotic zone, with Cycles 2 and 4 having lower mean temperature and higher mean nutrient concentrations (5–7 μM nitrate and 4–6 μM silicate) in the upper 20 m than other cycles, and coastal Cycle 1 being the only one with near-zero nitrate in the mixed layer (Table II).

Table I: Sampling dates, locations (initial and final) and depth ranges for experimental Cycles 1–5

		Initial		Final		
Experiment	Dates	Lat (°N)	Lon (°W)	Lat (°N)	Lon (°W)	Sample depths (m)
Cycle 1	23–27 June	9.72	87.00	9.56	86.72	2–90
Cycle 2	4–8 July	9.04	90.56	8.95	90.33	2–80
Cycle 3	9–13 July	10.42	92.92	9.83	92.92	2–100
Cycle 4	15–19 July	8.55	90.40	8.37	90.00	2–80
Cycle 5	20–24 July	8.88	88.46	9.53	87.43	2–100

Dates are local time, with daily early morning CTD casts at ~02:00.

Community biomass assessments

The mean cycle profiles for TChl *a* and total autotrophic carbon (AC) are plotted in Fig. 3. The mean values and error estimates (standard error of the mean) for the 4–5 profiles per cycle are given in Table II for mixed layer values and in Table III for depth-integrated biomass. Due to the emphasis on the open-ocean sampling sites and time and resources available for floristic analysis, microscopical estimates of carbon biomass are not available for the coastal Cycle 1.

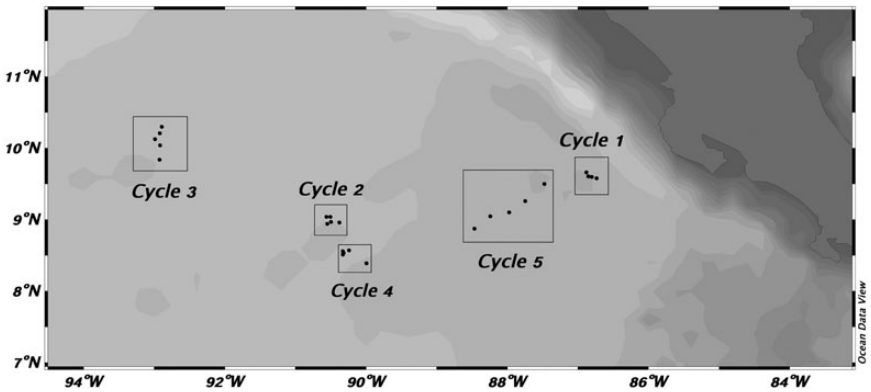

Fig. 1. Study region in the CRD area. Cycles indicate locations of sample collection during drifter experiments. Individual points within cycles indicate daily sampling.

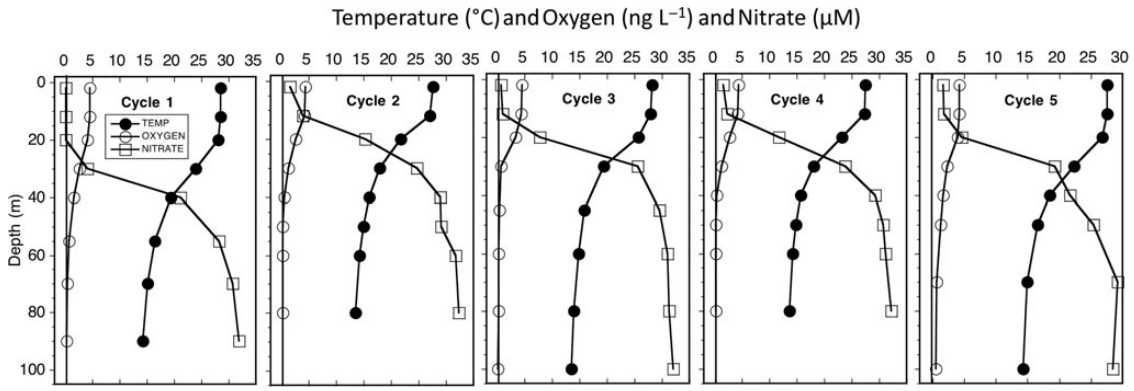

Fig. 2. Mean profiles of temperature (°C), dissolved oxygen (ng L^{-1}) and nitrate concentration (μM) for experimental Cycles 1–5.

Table II: Comparison of community and population-specific mean estimates of carbon biomass and taxon-specific accessory pigments for samples collected in the mixed-layer (upper 20 m) in the CRD in June–July 2010

Variable	Cycle 1	Cycle 2	Cycle 3	Cycle 4	Cycle 5
Temp (°C)	28.4 ± 0.1	25.5 ± 0.8	27.3 ± 0.3	26.0 ± 0.6	27.3 ± 0.2
Salinity	33.7 ± 0.1	33.9 ± 0.1	33.8 ± 0.1	33.8 ± 0.1	33.6 ± 0.0
Oxygen (mL L^{-1})	4.4 ± 0.1	3.7 ± 0.3	4.1 ± 0.2	3.8 ± 0.2	4.2 ± 0.1
Nitrate (μM)	0.09 ± 0.02	6.9 ± 1.8	3.1 ± 1.1	5.2 ± 1.5	2.7 ± 0.8
Silicate (μM)	1.0 ± 0.1	5.8 ± 1.0	2.8 ± 0.4	4.3 ± 0.7	2.9 ± 0.3
Carbon biomass—mixed layer (μg L^{-1})					
Sample # (*n*)	12	15	15	15	6
Community	ND	40.9 ± 3.4^{A}	25.0 ± 1.3^{a}	20.6 ± 2.2^{a}	28.3 ± 4.5
Synechococcus	10.2 ± 1.3	17.4 ± 2.4^{A}	7.5 ± 0.8^{a}	6.3 ± 0.9^{a}	6.1 ± 0.6^{a}
Prochlorococcus	2.7 ± 0.8	4.1 ± 0.4^{A}	1.3 ± 0.3^{a}	2.5 ± 0.4	2.3 ± 0.5
Pico-eukaryotes	ND	3.5 ± 0.4^{A}	3.3 ± 0.3^{B}	$1.3 \pm 0.3^{a,b}$	$1.0 \pm 0.2^{a,b}$
Diatoms	ND	0.2 ± 0.1^{A}	0.5 ± 0.2	0.6 ± 0.1^{a}	0.8 ± 0.3^{a}
Prymnesiophytes	ND	2.2 ± 0.2	2.0 ± 0.2	2.1 ± 0.3	3.2 ± 0.8
A-Dinoflagellates	ND	7.1 ± 0.8^{A}	6.8 ± 0.8^{B}	$4.1 \pm 0.5^{a,b}$	7.5 ± 1.9
A-Flagellates	ND	6.4 ± 0.8^{A}	3.6 ± 0.3	$3.6 \pm 0.7^{D,a}$	7.4 ± 1.7^{d}
Pigment concentration—mixed layer (ng L^{-1})					
Sample # (*n*)	12	14	15	15	15
Total Chl *a*	472 ± 53^{A}	399 ± 24^{B}	276 ± 16^{a}	$251 \pm 30^{a,b}$	$180 \pm 31^{a,b}$
MVChl *a*	408 ± 46^{A}	$308 \pm 14^{B,D}$	$251 \pm 14^{a,e}$	$212 \pm 26^{a,d}$	$157 \pm 15^{a,b,e}$
DVChl *a*	62 ± 12^{AD}	92 ± 11^{B}	24 ± 2^{b}	$27 \pm 5^{b,d}$	$13 \pm 1^{a,b}$
FUCO	56 ± 12^{A}	19 ± 2	24 ± 3	19 ± 4^{a}	11 ± 1^{a}
PER	24 ± 8	8 ± 1	10 ± 1	11 ± 2	8 ± 1
HEX	89 ± 15	123 ± 8^{D}	103 ± 10	85 ± 9	82 ± 10^{d}
BUT	27 ± 5	$46 \pm 8^{A,D}$	44 ± 8^{B}	25 ± 5^{d}	$17 \pm 2^{a,b}$
ZEAX	65 ± 11^{A}	113 ± 12^{B}	$34 \pm 3^{C,b}$	$28 \pm 4^{D,b}$	$11 \pm 2^{a,b,c,d}$

The upper table gives corresponding values for mixed-layer temperature, salinity, oxygen concentration and nitrate and silicate concentrations. All data are means ± standard errors (*n*, number of samples averaged). Superscript letters indicate a significant difference between means (Kruskal–Wallis, $P = 0.05$, followed by Dunn's test if a difference was found). The Dunn's test was first applied at a significance level of 0.05; if no significant difference was found, it was re-applied at $P = 0.10$. Superscripts A, B, C indicate significance at $P = 0.05$; D and E indicate $P = 0.10$. Upper- and lowercase letters show which cycle values differ (e.g. $Cyc1^{A}$; $Cyc5^{a}$ indicate that Cycles 1 and 5 differ at $P = 0.05$).
Variable abbreviations are: A, autotroph; MVChl *a*, monovinyl chlorophyll *a*; DVChl *a*, divinyl chlorophyll *a*; FUCO, fucoxanthin; PER, peridinin; HEX, 19′-hexanoyloxyfucoxanthin; BUT, 19′-butanoyloxyfucoxanthin; ZEAX, zeaxanthin; ND, no data.

The data highlight a 2-fold difference in mixed-layer biomass, with significantly higher TChl *a* (≥400 ng L^{-1}) for Cycles 1 and 2 ($P = 0.05$), and significantly higher mean AC for Cycle 2 (40.9 ± 3.4 μg C L^{-1}) in the central dome area ($P = 0.05$), relative to the other open-ocean cycles (Table II). The mean integrated estimates carbon biomass also exhibit <2-fold variability, with the highest estimate for Cycle 2 (1.86 g C m^{-2}), lowest values for Cycles 3 and 4 (1.1 g C m^{-2}) and intermediate estimate for Cycle 5 (1.6 g C m^{-2}) (Table III). Among the open-ocean sites

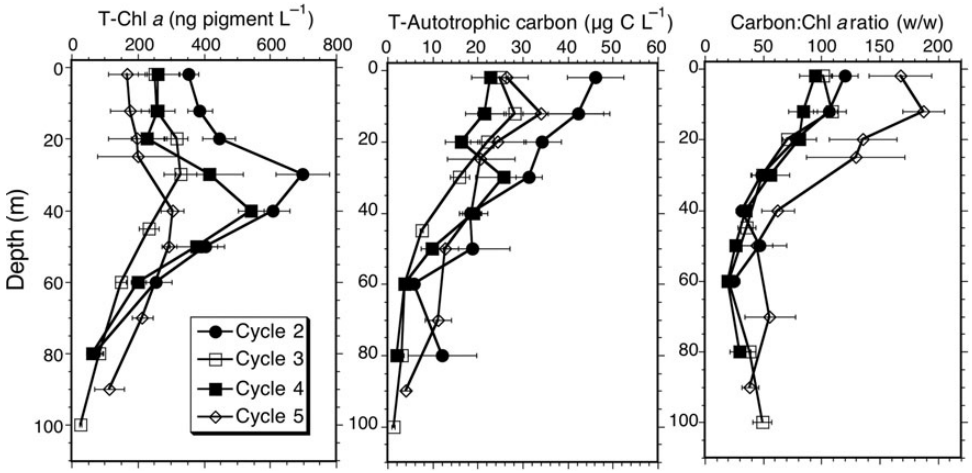

Fig. 3. Depth profiles for TChl *a*, total autotrophic carbon biomass and carbon:TChl *a* ratios for the phytoplankton communities sampled during experimental Cycles 2–5. Symbols are means ± standard errors. The Kruskal–Wallis non-parametric ANOVA tests indicated that the means for TChl *a* at 20, 30 and 40 m were significantly different among cycles ($P = 0.05$), but *post hoc* Dunn tests failed to confirm differences among cycle means.

Table III: Comparison of euphotic zone-integrated estimates of community and population-specific carbon biomass and pigment concentrations in the CRD during June–July 2010

Variable	Cycle 1	Cycle 2	Cycle 3	Cycle 4	Cycle 5
Mixed layer (m)	23.8 ± 0.9	18.7 ± 1.4	21.1 ± 0.8	20.5 ± 1.9	30.9 ± 2.7
20°C isotherm	43.1 ± 0.8	26.4 ± 1.6	32.6 ± 0.5	31.6 ± 3.2	42.3 ± 2.9
1% light level	45.9 ± 0.6	44.6 ± 1.0	52.1 ± 1.4	49.7 ± 1.9	56.7
Carbon biomass—euphotic zone (mg m^{-2})					
Sample # (*n*)	4	5	5	5	2
Community	ND	1858 ± 185^{A}	1089 ± 57^{a}	1102 ± 144^{a}	1593 ± 340
Synechococcus	355 ± 101	651 ± 101^{A}	216 ± 18^{a}	339 ± 38	183 ± 67
Prochlorococcus	104 ± 29	252 ± 37^{A}	99 ± 22^{a}	220 ± 56	152 ± 87
Pico-eukaryotes	ND	171 ± 20	191 ± 24^{A}	72 ± 16^{a}	82 ± 27
Diatoms	ND	7 ± 2^{D}	19 ± 7	20 ± 5	31 ± 1^{d}
Prymnesiophytes	ND	102 ± 9	113 ± 11	102 ± 11	212 ± 86
A-Dinoflagellates	ND	380 ± 93^{A}	256 ± 21	175 ± 24^{a,B}	479 ± 47^{b}
A-Flagellates	ND	298 ± 40	195 ± 9	175 ± 32	454 ± 120
Pigment concentration—euphotic (mg m^{-2})					
Sample # (*n*)	4	5	5	5	5
Total Chl *a*	37.3 ± 5.7^{A}	31.2 ± 1.0^{B,D}	19.1 ± 1.0^{a,d}	23.3 ± 1.0	17.0 ± 2.2^{a,b}
MVChl *a*	31.1 ± 4.3^{A,D}	19.7 ± 0.6	15.0 ± 0.8^{d}	14.5 ± 0.6^{a}	14.2 ± 1.8^{a}
DVChl *a*	6.2 ± 1.5	11.4 ± 0.7^{A}	4.1 ± 0.4^{a}	8.8 ± 0.5	2.9 ± 0.5^{a}
FUCO	4.7 ± 0.8^{A,D}	2.5 ± 0.2^{E}	2.2 ± 0.4	1.7 ± 0.1^{d}	1.4 ± 0.1^{a,e}
PER	2.4 ± 0.8^{A,D}	0.6 ± 0.1^{a}	0.6 ± 0.1^{d}	0.6 ± 0.1^{d}	0.8 ± 0.1
HEX	7.3 ± 0.7^{A}	6.2 ± 0.5	4.8 ± 0.5	4.2 ± 0.3^{a}	6.1 ± 1.1
BUT	3.0 ± 0.5	3.3 ± 0.5	3.2 ± 0.3	2.1 ± 0.1	3.2 ± 0.4
ZEAX	2.6 ± 0.8	5.1 ± 0.4^{A}	1.3 ± 0.1^{a}	2.1 ± 0.2	0.7 ± 0.1^{a}

Upper table gives corresponding values for mixed-layer depth (m), depth of the 20°C isotherm (m) and the depth of 1% of surface irradiance (m). All data are means ± standard errors (*n*, number of samples averaged). Superscript letters indicate a significant difference between means (Kruskal–Wallis, $P = 0.05$, followed by Dunn's test if a difference was found). Significance levels and variable abbreviations as in Table II.

where the biomass ratio of AC:TChl *a* could be determined, the results show close agreement for Cycles 2–4, which all have mean values in the range of 82–102 for the upper 20 m (Table II), and decline similarly with depth (Fig. 3) to give the mean euphotic zone values of 47–60 (Table III). Significantly, higher AC:Chl *a* ratios for Cycle 5 extend throughout the profile. This ratio anomaly appears to come from low TChl *a* values for Cycle 5 rather than phytoplankton carbon biomass, which is in the range measured for other cycles (Fig. 3). For the 17 euphotic-zone profiles in which both AC and TChl *a* were measured contemporaneously, the cruise mean values (± SE) for depth-integrated

AC, TChl *a* and C:Chl are 1378 ± 112 mg C m^{-2}, 24.1 ± 1.5 mg Chl *a* m^{-2} and 57.5 ± 3.4, respectively.

Phytoplankton size structure

Size structure analysis for the phytoplankton community illustrates the importance of picophytoplankton in the CRD region (Fig. 4). Picophytoplankton dominance was highest for Cycles 2 and 4, with <2 μm cells accounting for ~60% of carbon biomass in the central dome region and a slightly lower proportion (~50%) on the dome fringe for Cycle 3. Micro-sized phytoplankton (cells >20 μm) accounted for typically ~10% or less of phytoplankton biomass in all of the open-ocean sampling areas (Fig. 4). Overall, Cycles 2–4 show strong similarity in relative size structure, despite their 2-fold difference in total biomass. Size structure for Cycle 5 is quite different, however, with nanophytoplankton rather than picophytoplankton accounting for the majority (>60%) of total community carbon. In comparing the different size categories between cycles (Kruskal–Wallis test) at $P = 0.05$, only the higher A-NANO in Cycle 4 relative to Cycle 5 is significant. However, if a lower significance level of $P = 0.10$ is used, then A-PICO is higher in Cycle 2 than Cycle 3, A-NANO is highest in Cycle 5 and A-NANO and A-MICRO are both significantly higher in Cycle 2 than in Cycle 4.

Phytoplankton composition

Phytoplankton group contributions to community carbon biomass and mean values of taxon-associated accessory pigments are given for the upper 20 m in Table II and as depth-integrated values in Table III. Among the picophytoplankton, SYN comprised over 40% (17.4 μg C L^{-1}) of near-surface phytoplankton carbon for Cycle 2 in the core dome region, with contributions declining in waters further away from the core (e.g. ~30% for Cycles 3 and 4; ~20% for Cycle 5). We did however measure relatively high abundances and carbon biomass for SYN in surface waters in the coastal Cycle 1. PRO made significant contributions to biomass (1.3–4.1 μg C L^{-1}), although always less than SYN, at all sampling locations, and P-Euk estimates (1.0–3.5 μg C L^{-1}) were similar to, although usually less, than those for PRO for all sites compared (Table II). For integrated carbon values, PRO showed a similar pattern. On the whole, good relationships were observed between PRO carbon and its diagnostic pigment DVChl *a*, both showing strong subsurface maxima below the mixed layer for Cycles 2 and 4 in the dome area and more uniform depth profiles for Cycles 1, 3 and 5 (Fig. 5). The slight subsurface pigment maxima observed for these latter cycles reflect photoacclimation of cellular pigment content, and are not seen as abundance or biomass peaks. For the cyanobacteria-associated photoprotective pigment zeaxanthin, cycle differences in SYN biomass are reflected in proportional variations of ZEAX concentrations and depth-integrated values (Tables II and III, Fig. 5).

Among major eukaryote groups of phytoplankton, diatoms contributed variable amounts but relatively little overall (maximally ~1 μg C L^{-1}) to community carbon. Maximal values were seen in surface samples for dome Cycles 2 and 4 and at 20 m for Cycle 3 and 5, and diatom biomass was notably lower for dome core Cycle 2 relative to the other locations (Fig. 6). Biomass estimates for prymnesiophytes (Prym) were similar (mixed layer values ~2 μg C L^{-1}) for Cycles 2–4, but Cycle 5 gave estimates about 1.5 times higher. The dominant carbon contributions among eukaryotic groups come by far from dinoflagellates (A-Dino) and other unidentified flagellates

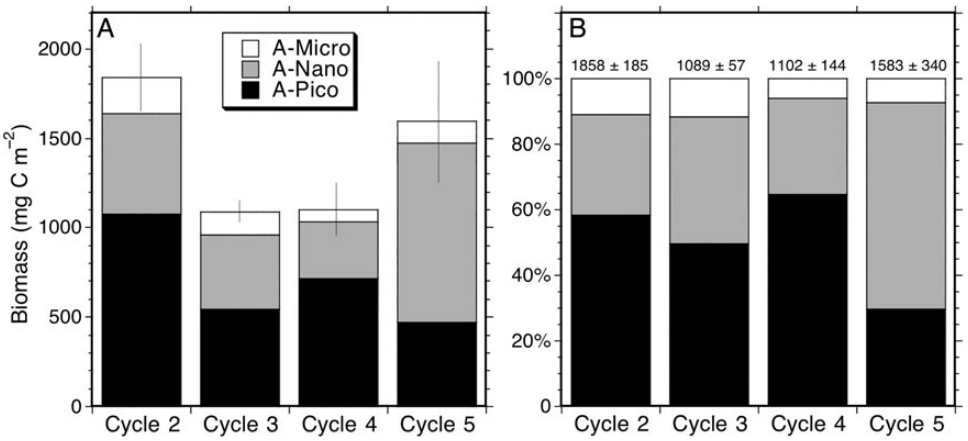

Fig. 4. Phytoplankton community size structure for experimental Cycles 2–5. (**A**) Mean carbon biomass of Pico (<2 μm), Nano (2–20 μm) and Micro (>20 μm) sized cells. (**B**) Percentage contributions of the size classes to total community carbon. Error bar in A is standard error of the total community estimate. The mean community carbon biomass and standard errors are given above histograms at the top of B.

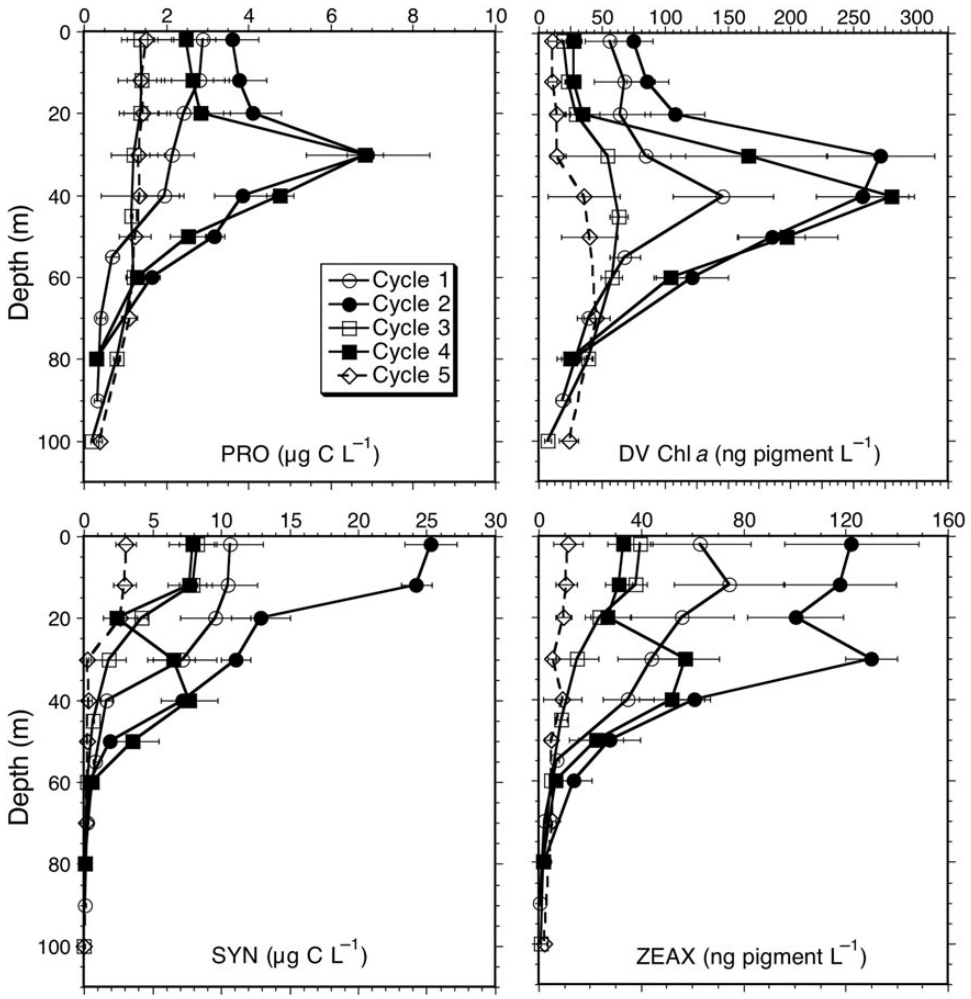

Fig. 5. Mean depth profiles of carbon biomass for *Prochlorococcus* (PRO) and *Synechococcus* (SYN) and pigment concentrations for divinyl Chl *a* (DV Chl a) and zeaxanthin (ZEAX) from experimental Cycles 1–5. Integrated values for ZEAX and DVChl were significantly different for Cycles 2, 3 and 5 (Kruskal–Wallis and Dunn's tests, $P = 0.05$; Table III). Error bars are standard errors of mean estimates.

(A-Flag), each contributing more than Diat and Prym combined for all cycles (Tables II and III). Biomass estimates for these groups are relatively high for Cycle 2, but lowest for Cycle 4, showing substantial variability within the central dome region, comparable to that among all cycles in and out of the dome (Fig. 6).

Eukaryote-associated accessory pigments were relatively similar for Cycles 2–4, so these cycles are averaged together in Fig. 7 to emphasize differences with respect to out-of-dome Cycles 1 and 5. MV Chl *a* profiles show that Cycle 2–4 values are intermediate between Cycles 1 and 5, and do not display the strongly elevated subsurface concentrations seen in coastal Cycle 1 where nutrients were highly depleted in the mixed layer. All cycles show the highest accessory pigment concentration for HEX throughout the depth profiles, and generally the lowest values for PER, the exception being the subsurface maximum in PER (>120 ng L^{-1}) at 30 m in Cycle 1 (Fig. 7). BUT has a similar profile in Cycle 1 and in the Cycles 2–4 average, both showing subsurface maxima (~70 ng L^{-1}) at ~30 m, about double the near-surface values. For Cycle 5, however, BUT concentrations are lower and extend deeper without a prominent subsurface maximum. FUCO is a significant pigment, second to HEX, in the profiles for coastal Cycle 1, but less so for combined Cycles 2–4 and especially for Cycle 5.

Carbon and pigment-based assessments of community composition are compared in Fig. 8, which includes computations of group-specific contributions to TChl *a* from the tabulated raw pigment concentrations (Tables II and III) following the approach of Goericke and Montoya (Goericke and Montoya, 1998). The carbon-based compositional analysis mainly reiterates what was revealed above. SYN is the dominant biomass contributor among the prokaryotes and

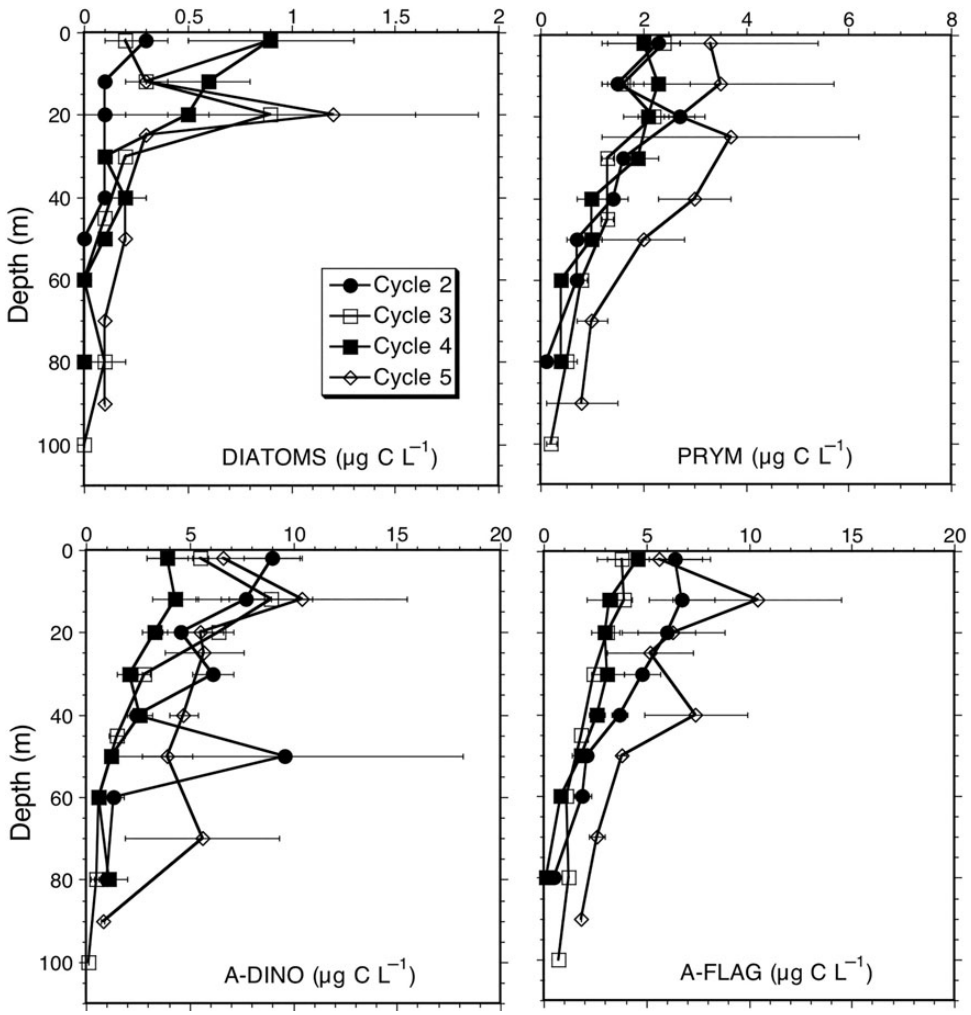

Fig. 6. Mean depth profiles of eukaryote carbon biomass (µg C L^{-1}) for experimental Cycles 1–5. Categories are diatoms, prymnesiophytes (Prym), autotrophic dinoflagellates (A-Dino) and unidentified autotrophic flagellates (A-Flag). Error bars are standard errors of the mean.

picophytoplankton, while A-Flag and A-Dino are the dominant contributors among eukaryotic phytoplankton. Diatoms are notably low in results for all sampling locations. The pigment-based analysis includes other groups like pelagophytes (Pelago) and chlorophytes (Chloro) that could not be distinguished by EPI microscopy, or which were observed in very low numbers (Crypto) and therefore grouped with A-Flag. EPI + FCM and pigment-based results indicate that autotrophic picoplankton (A-PICO) are the dominant contributors to phytoplankton carbon (Fig. 8). Specifically, EPI + FCM results show that the biomass from SYN, PRO and small eukaryotes (A-FLAG), such as Pelago (assumed as part of A-FLAG that cannot be distinguish by EPI) and Prym (can only distinguish a portion of the total population by EPI, the rest are in A-FLAG), is >50% for each cycle (Fig. 8A). Supporting this are pigment-based results showing that >50% of TChl *a* is associated with smaller taxa (Fig. 8B). Among larger eukaryotic taxa, however, there are significant discrepancies in the inferences of composition that come from the pigment-based analysis compare to microscopy. Most notably, the pigments suggest a 5- to 10-fold greater contribution from DIAT than is evident in carbon biomass, and the contribution of A-Dino are underestimated by more than an order of magnitude in some cases (e.g. Cycle 2) relative to carbon-based assessments (Fig. 8).

DISCUSSION

Phytoplankton variability in the CRD

Although the sampling locations in this study were not broadly dispersed in the CRD area, we were able to compare phytoplankton stocks across a range of conditions,

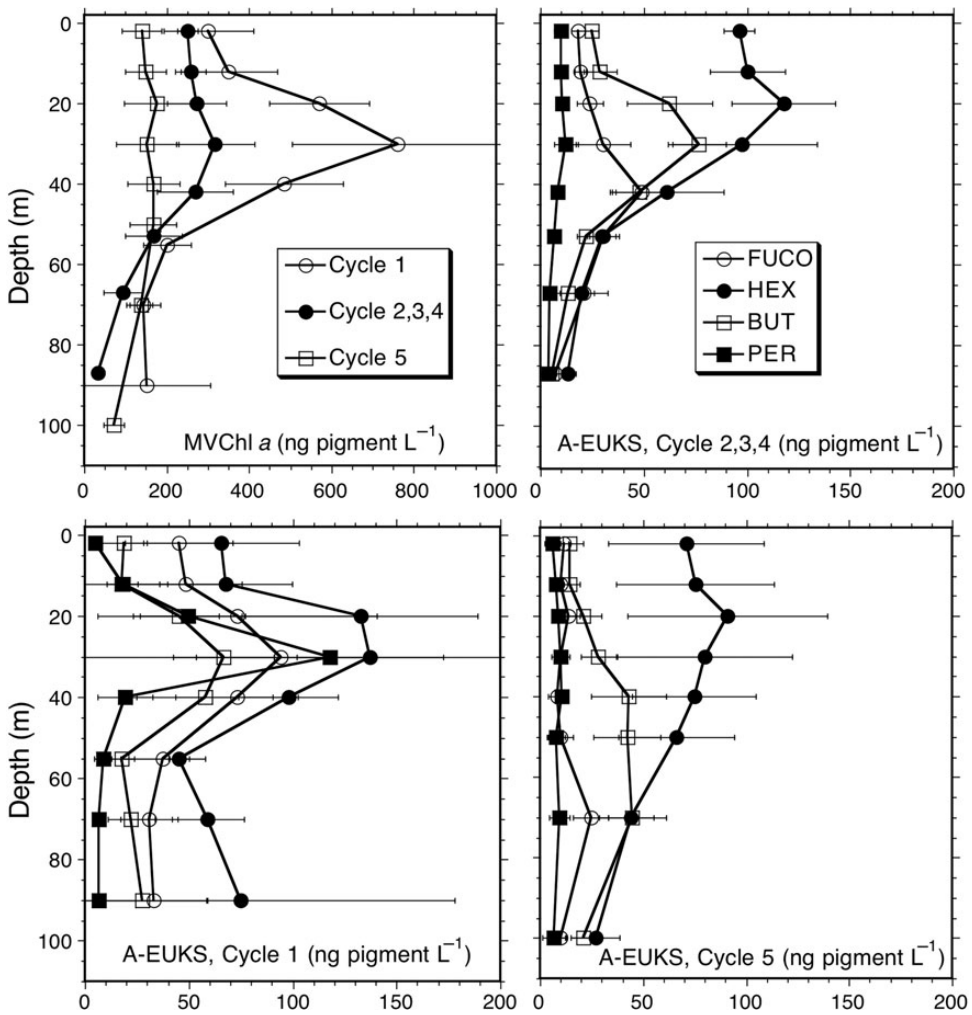

Fig. 7. Depth profiles of eukaryote-associated pigment concentrations (ng L^{-1}) for experimental Cycles 1–5. Categories are monovinyl Chl *a* (MVChl*a*), fucoxanthin (FUCO), hexfucoxanthin (HEX), butfucoxanthin (BUT) and peridinin (PER). Integrated values were not significantly different for Cycles 2–4 (Table III), which are grouped in this plot. Differences were significant for some pigments between Cycles 1 and 5, which are plotted separately. Error bars are standard errors of mean estimates.

including open-ocean waters of the central dome region, at the outer dome edge, in the North Equatorial Counter Current, and in more coastal waters. Despite this site variety, we found the differences in the mean standing stock estimates among cycles to be substantially less than order-of-magnitude and more like a factor of 2 or 3 range for most variables measured (Tables II and III). To break this down further, the semi-Lagrangian sampling design allows us to compare variability among cycle experiments (inter) to variability within cycles (intra), i.e. from repeated daily sampling of water parcels marked with a satellite-tracked drifter. For this, we focus on the community-level biomass assessments for total AC and TChl *a*, as well as PRO and SYN, the major picophytoplankton populations enumerated very precisely by flow cytometry.

For total AC, the coefficient of variation (CV) for intra-cycle sampling was only slightly lower than for inter-cycle values for the integrated water column (22 versus 27%, respectively), while the intra-cycle CV was even higher than found for inter-cycle variability for 0–20 m sampling (37 versus 29%, respectively). Similarly, intra-cycle CVs were consistently lower than inter-cycle CVs for SYN (50 versus 57% for 0–20 m sampling; 33 versus 53% for integrated values), but consistently higher than inter-cycle CVs for PRO (63 versus 42% for 0–20 m sampling; 54 versus 42% for integrated values) and generally similar to inter-cycle CVs for TChl *a* (36 versus 41% for 0–20 m sampling; 22 versus 27% for integrated values). Our conclusion from these comparisons, that within-cycle sampling variability was generally quite high and similar to variability seen among the different experimental cycles, is

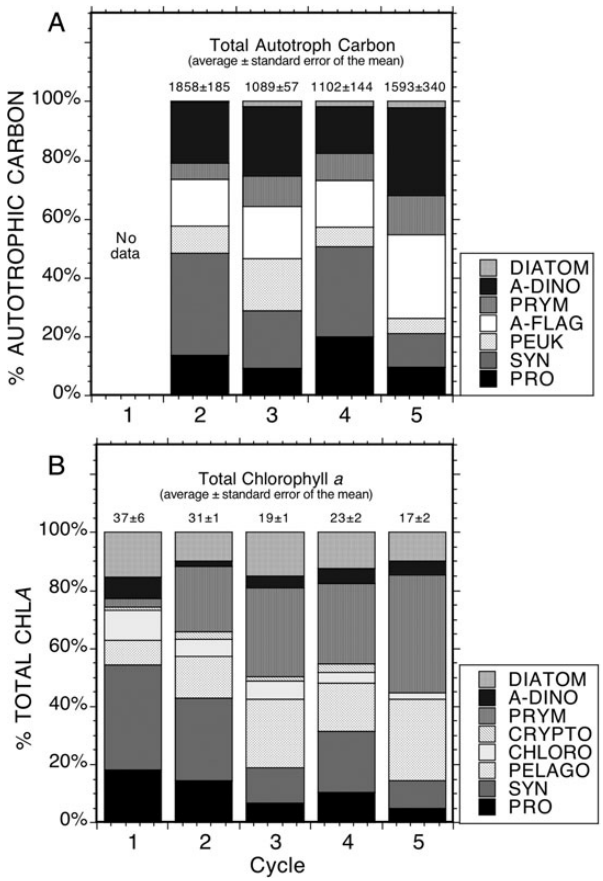

Fig. 8. Comparison of group-specific composition of the phytoplankton community in terms of (**A**) group contributions to depth-integrated carbon biomass and (**B**) group contributions to total depth-integrated Chl *a* from HPLC pigment analyses. Mean values ± standard errors for experimental cycles are given at the top of each histogram.

consistent with the impression that we had made during the cruise based on daily FCM counting on shipboard. It seems surprising that this should be so, especially for near-surface sampling, as the drift array was designed with a very substantial holey-sock drogue (1 m diameter × 3 m long) centered at 15 m to follow mixed-layer water, and daily sampling was done as close as could be safely done relative to the drifter position. Abrupt community changes were nonetheless noted in daily results that seem to reflect real small-scale spatial variability (≤100 s to 100 s m) relative to the drifter. Particularly in the central dome region, drifter paths exhibited strong oscillatory excursions associated with inertial tides (Landry *et al.*, 2016a), which may lead to temporal and spatial variability in nutrient delivery and patches or streaks or water with different nutrient upwelling histories. In addition, the water-column currents were strongly sheared such that, even following a mixed-layer drifter, the upper 15–20 m waters were interacting with continuously changing nutrient sources waters directly below which arrived from different directions and at different speeds. Such conditions might reasonably create a diverse mosaic of small-scale habitats for the phytoplankton community, which is captured in the daily sampling variability.

The similarities observed in intra- and inter-cycle sampling variability during this study must also be interpreted in the context of apparently atypical physical conditions in the CRD during summer 2010. The Eastern tropical Pacific experienced moderate El Niño conditions during the winter and spring prior to the cruise, and even though that was changing at the time of the cruise, summer 2010 stands out as the only one in a decade of satellite measurements analyzed without a significant summertime increase in surface Chl *a* to distinguish the CRD waters from the open-ocean waters around it (Landry *et al.*, 2016a). For example, while surface Chl *a* appeared to remain at background low levels throughout summer 2010, the adjacent years (2009 and 2011) each achieved mid-summer peaks in excess of 1.5 mg Chl *a* m^{-3}, averaged from MODIS-Aqua imagery for the area of 8–11°N, 88–93°W (Landry *et al.*, 2016a). Peak summertime values for the same area in 2013 were >3.5 mg Chl *a* m^{-3}. It is therefore likely that the ranges observed in phytoplankton biomass and composition in and out of dome waters during 2010 were not representative of what they might be for a more fully developed CRD in a normal summer.

Community characteristics of CRD phytoplankton

The present study supports previous conclusions that picophytoplankton, and SYN in particular, are major contributors to phytoplankton biomass in the CRD (Li *et al.*, 1983; Saito *et al.*, 2005; Ahlgren *et al.*, 2014). As possibly a result of suppressed CRD conditions in summer 2010, the highest SYN abundances that we found (~3×10^5 cells mL^{-1}) were an order of magnitude lower than the reported previously maximum (Saito *et al.*, 2005). Nonetheless, SYN alone accounted for almost half of the total AC estimated in the upper 20 m during Cycle 2, and 35% of the depth-integrated carbon in the central dome area (Tables II and III). With PRO and P-Euk also making significant contributions at all locations sampled, total picophytoplankton typically comprised the majority of community biomass in the dome-associate cycles (Cycles 2–4; Fig. 4).

What distinguishes this study from previous analyses of phytoplankton in the CRD is that we extend a carbon-based analysis to the whole phytoplankton community. Li *et al.* (Li *et al.*, 1983), for example, used size-fractionated Chl *a* to assess picophytoplankton contribution to the total, assuming and a C:Chl *a* ratio of 40 for carbon

conversions. Saito *et al.* (Saito *et al.*, 2005) compared FCM-based estimates of SYN carbon to measured POC in surface waters, and used biogenic silica and an assumed C:Si ratio to estimate diatom C, while Franck *et al.* (Franck *et al.*, 2003) from the same cruise reported diatom cell counts from a shipboard incubation experiment, but no carbon estimates. Lastly, Ahlgren *et al.* (Ahlgren *et al.*, 2014) recently reported the first eukaryotic carbon biomass estimates for the CRD, based on FCM cell counts (no size determinations) and an assumed fixed conversion factor of 1500 fg C cell^{-1}. In the present results, it is clear that phytoplankton community biomass averages >1 g C m^{-2} throughout the region and can exceed 2.4 g C m^{-2} in the central dome region even in a suppressed upwelling year. While diatoms are low, there are substantial biomass contributions of larger flagellates and dinoflagellates, as well as the productivity from and grazing on them (Décima *et al.*, 2016; Freibott *et al.*, 2016; Landry *et al.*, 2016b), to support a food web with high standing stocks of mesozooplankton and larger predators. These results thus give broader insight into how the CRD region can be picophytoplankton dominated yet still function trophically.

While carbon biomass estimates can be derived quite easily from measured Chl *a* values, our data also illustrate that such interpretations can be tricky. For example, the commonly used C:Chl *a* conversion factor of 50 would underestimate surface phytoplankton biomass estimates by about half relative to what we measured. If only FCM estimates of picophytoplankton carbon were then compared with such estimates, it might reasonably appear as if there was little biomass of large phytoplankton in the CRD upon which mesozooplankton could feed directly.

Comparison of FCM and EPI-derived carbon biomass estimates to pigment biomass proxies from group-specific HPLC analyses also highlights some concerns about how pigment estimates are used here and elsewhere. The picophytoplankton proxies emerge as relatively informative in this comparison since DV Chl *a* is uniquely associated with PRO and because SYN is so important that it dominates the ZEAX signal. Since we did not size-fractionate the pigments, it is difficult to match BUT and HEX to the respective contributions of pelagophytes and prymnesiophytes to pico- and nano-autotroph biomass, but overall inferences from these pigment seem to be consistent with realistic roles of those two phytoplankton groups in the phytoplankton community. That is not the case, however, for the diatom-proxy FUCO and the dinoflagellate-proxy PER, which grossly over- and underestimated, respectively, those group contributions to community carbon. The latter is a well-known problem in community analyses for open-ocean systems (e.g. Andersen *et al.*, 1996; Landry *et al.*, 2000; Selph *et al.*, 2011; Taylor *et al.*, 2011), where the major dinoflagellate lineages must presumably be among those with accessory pigments other than PER (Tangen and Björnland, 1981; Jeffrey and Wright, 2005). Here we can see, however, that the very low PER concentrations in the CRD give an order-of-magnitude distortion of the likely role of dinoflagellates in that system, notably as a resource of larger cells for larger planktonic consumers. By the same token, the distorted perspective on diatom importance from measured FUCO concentrations suggests that much of that pigment may reside in other groups, possibly A-Dino and Prym. This situation is probably unusual for an upwelling system, where diatoms typically dominate biomass and therefore the FUCO signal. Nonetheless, it is a caution against over-interpreting biomass, growth and grazing results based on FUCO as strictly diatom-related in systems like the CRD, where diatoms are relatively scarce.

Comparisons to phytoplankton in the central and equatorial Pacific

The CRD region resides in the southeastern sector of the North Pacific adjacent to the Eastern Equatorial Pacific (EEP) and the North Pacific Subtropical Gyre (NPSG). These systems, while ecologically distinct, are in sufficiently close proximity with fluid boundaries and current systems to allow for relatively easy population seeding and exchange among them. What we therefore observe as similarities and differences in their phytoplankton communities are important not only for describing the system characteristics but also for providing insights into the net selective effects of their different growth mortality environments.

In both the CRD and EEP, upwelling injects nutrients into the base of the euphotic zone, enhancing concentrations of Chl *a*, phytoplankton abundance and biomass compared with the surrounding oligotrophic open-ocean environments like the NPSG. While the roles of different elemental limitations, including cobalt (Saito *et al.*, 2005; Ahlgren *et al.*, 2014) silica, zinc and iron (Franck *et al.*, 2003; Chappell *et al.*, 2016; Goes *et al.*, 2016), are not yet fully resolved for CRD phytoplankton, iron is the demonstrated limiting resource in the EEP (Murray *et al.*, 1994; Coale *et al.*, 1996; Brzezinski *et al.*, 2011). Despite these potential limitation differences, integrated autotrophic carbon biomass (1378 $\pm$ 112 mg C m^{-2}) and depth-averaged concentrations (16 $\pm$ 1.5 μg C L^{-1}) for the CRD region are very similar to values in the EEP (1369 $\pm$ 54 mg C m^{-2} and 14.8 $\pm$ 4.2 μg C L^{-1}, respectively), based on 31 stations sampled between 4°N and 4°S, 110 to 140°W as part of the Equatorial Biocomplexity (EB) project (Nelson and Landry, 2011; Taylor *et al.*, 2011). In both areas, though

possibly an anomaly for the CRD in summer 2010, phytoplankton community biomass was fairly consistent throughout the region, varying by only a factor of 2.7 in EB. C:Chl ratios averaged 90 in our CRD data for the mixed layer and 57 for the full water column. Results for the EEP were lower (78) for the mixed layer but comparable (64) for the integrated water column (Taylor *et al.*, 2011), potentially reflecting compositional differences or different trace-element limitations that mainly impact cells in the mixed layer.

Beneath their bulk carbon similarities, the CRD and EEP differ appreciably in community composition and size structure. While picophytoplankton clearly dominate size in the CRD, A-Nanos account for almost half (46%) of community biomass in the EEP, followed by A-Pico (39%) and A-Micro (16%). In the EEP as well as in the NPSG, PRO rather than SYN is the picophytoplankton dominant (Landry and Kirchman, 2002). Iron limitation by itself thus does not alter the dominance pattern of PRO in oligotrophic waters, though higher standing stocks of SYN and P-Euks than generally occur in NPSG are superimposed on PRO in the EEP (Landry and Kirchman, 2002). The CRD and EEP also differ in the relative roles of diatoms, with diatom contributions to biomass and production being about an order of magnitude lower in the CRD (Landry *et al.*, 2011, 2016b; Taylor *et al.*, 2011; Krause *et al.*, 2016).

One shared characteristic of the CRD and EEP upwelling regions is the importance of A-Dino, when compared with the NPSG, where they make up a much smaller portion of the autotrophic community (Brown *et al.*, 2008; Pasulka *et al.*, 2013). In the EEP region, A-Dino account for an extraordinary 39% of AC, when compared with 23% for the CRD. A-Dino dominate the nano- and micro-phytoplankton size classes in both the CRD and EEP. As noted previously, A-Dino importance in both regions is also vastly underestimated by pigment proxies.

One hypothesis for the dominance of typically slower growing A-Dinos in these open-ocean upwelling regions is that they might benefit from mixotrophic nutritional strategy when competing with other smaller phytoplankton for limiting resources (Sanders, 1991; Jacobson and Anderson, 1996; Stoecker, 1999). With demonstrated iron-limitation in the EEP (Coale *et al.*, 1996; Brzezinski *et al.*, 2011) and likely trace-element limitation in the CRD (Franck *et al.*, 2003), the ability to acquire trace metal and iron resources by phagotrophy (i.e. eating smaller competitors) could explain the relative success of A-Dinos in these systems. The lesser importance of A-Dinos in major nutrient (nitrogen and phosphorous) limited systems, such as the NPSG could mean that mixotrophy is not as efficient in satisfying bulk nutrient and carbon requirements for growth as it is in acquiring trace elements.

The biomass similarities but compositional distinctness of CRD and EEP regions and the shortcomings of pigment proxies speak to the difficulties of interpreting phytoplankton community structure much less dynamics from remotely sensed satellite or *in situ* optical methods (e.g. Mouw and Yoder, 2005). Care must be taken when applying broad-scale algorithms to regions such as the CRD, and additional research should be conducted to further elucidate and understand the complex interactions and dynamics with microbial communities in the CRD upwelling dome.

ACKNOWLEDGEMENTS

We thank the captain, crew and research technicians of the R/V Melville, whose efforts contributed significantly to the success of the cruise. We also gratefully acknowledge the specific help of Daniel Wick, John Wokuluk, Megan Roadman and Ally Pasulka with sample collections, preparations and analyses on sea and land.

FUNDING

This component of the CRD Flux and Zinc Experiments project was supported by US National Science Foundation grant OCE-0826626 to M.R.L.

DATA ARCHIVING

Cruise data are available through the Biological and Chemical Oceanography Data Management Office under the project title "Costa Rica Dome Flux and Zinc Experiments" (http://www.bco-dmo.org/project/515387).

REFERENCES

Ahlgren, N. A., Noble, A., Patton, A. P., Roache-Johnson, K., Jackson, L., Robinson, D., McKay, C., Moore, L. R. *et al.* (2014) The unique trace metal and mixed layer conditions of the Costa Rica upwelling dome support a distinct and dense community of *Synechococcus*. *Limnol. Oceanogr.*, **59**, 2166–2184.

Andersen, R. A., Bidigare, R. R., Keller, M. D. and Latasa, M. (1996) A comparison of HPLC pigment signatures and electron microscopic observations for oligotrophic waters of the North Atlantic and Pacific Oceans. *Deep-Sea Res. II*, **43**, 517–537.

Ballance, L. T., Pitman, R. L. and Fiedler, P. C. (2006) Oceanographic influences on seabirds and cetaceans of the eastern tropical Pacific: A review. *Prog. Oceanogr.*, **69**, 360–390.

Bidigare, R. R. and Ondrusek, M. E. (1996) Spatial and temporal variability of phytoplankton pigment distributions in the central equatorial Pacific Ocean. *Deep-Sea Res. II*, **43**, 809–833.

Binder, B. J., Chisholm, S. W., Olson, R. J., Frankel, S. I. and Worden, A. Z. (1996) Dynamics of picophytoplantkon, ultraphytoplankton and bacteria in the central equatorial Pacific. *Deep-Sea Res. II*, **43**, 907–931.

Blackburn, M., Laurs, R. M., Owen, R. W. and Zeitzschel, B. (1970) Seasonal and areal changes in standing stocks of phytoplankton, zooplankton and micronekton in the eastern tropical Pacific. *Mar. Biol.*, **7**, 14–31.

Brown, S. L., Landry, M. R., Neveux, J. and Dupouy, C. (2003) Microbial community abundance and biomass along a 180° transect in the equatorial Pacific during an El Niño-Southern Oscillation cold phase. *J. Geophys. Res.*, **108**, 8139. doi:10.1029/2000JC000817.

Brown, S. L., Landry, M. R., Selph, K. E., Yang, E. J., Rii, Y. M. and Bidigare, R. R. (2008) Diatoms in the desert: plankton community response to a mesoscale eddy in the subtropical North Pacific. *Deep-Sea Res. II*, **55**, 1321–1333.

Brzezinski, M. A., Baines, S. B., Balch, W. M., Beucher, C. P., Chai, F., Dugdale, R. C., Krause, J. W., Landry, M. R. *et al.* (2011) Co-limitation of diatoms by iron and silicic acid in the equatorial Pacific. *Deep-Sea Res. II*, **58**, 493–511.

Campbell, L. and Vaulot, D. (1993) Photosynthetic picoplankton community structure in the subtropical North Pacific Ocean near Hawaii (station ALOHA). *Deep-Sea Res. I*, **40**, 2043–2060.

Chappell, P. D., Vedmati, J., Selph, K. A., Cyr, H. A., Jenkins, B. D., Landry, M. R. and Moffett, J. W. (2016) Preferential depletion of zinc within Costa Rica Upwelling Dome creates conditions for zinc co-limitation of primary production. *J. Plankton Res.*, **38**, 244–255.

Chavez, F. P., Buck, K. R., Service, S. K., Newton, J. and Barber, R. T. (1996) Phytoplankton variability in the central and eastern tropical Pacific. *Deep-Sea Res. II*, **43**, 835–870.

Coale, K. H., Johnson, K., Fitzwater, S. E., Gordon, R. M., Tanner, S. A., Chavez, F. P., Ferioli, L., Sakamoto, C. *et al.* (1996) A massive phytoplankton bloom induced by an ecosystem-scale iron fertilization experiment in the equatorial Pacific Ocean. *Nature*, **383**, 495–501.

Décima, M., Landry, M. R., Stukel, M. R., López-López, L. and Krause, J. W. (2016) Mesozooplankton biomass and grazing in the Costa Rica Dome: amplifying variability through the plankton food-web. *J. Plankton Res.*, **38**, 317–330.

Fiedler, P. C. (2002) The annual cycle and biological effects of the Costa Rica Dome. *Deep-Sea Res. I*, **49**, 321–338.

Fiedler, P. C., Philbrick, V. and Chavez, F. P. (1991) Oceanic upwelling and productivity in the eastern tropical Pacific. *Limnol. Oceanogr.*, **36**, 1834–1850.

Franck, V. M., Bruland, K. W., Hutchins, D. A. and Brzezinski, M. (2003) Iron and zinc effects on silicic acid and nitrate uptake kinetics in three high-nutrient, low-chlorophyll (HNLC) regions. *Mar. Ecol. Prog. Ser.*, **252**, 15–33.

Freibott, A., Taylor, A. G., Selph, K. E., Liu, H., Zhang, W. and Landry, M. R. (2016) Biomass and composition of protist grazers and heterotrophic bacteria in the Costa Rica Dome during summer 2010. *J. Plankton Res.*, **38**, 230–243.

Garrison, D. L., Gowing, M. M., Hughes, M. P., Campbell, L., Caron, D. A., Dennett, M. R., Shalapyonok, A., Olson, R. J. *et al.* (2000) Microbial food web structure in the Arabian Sea: a US JGOFS study. *Deep-Sea Res. II*, **47**, 1387–1422.

Goericke, R. (2002) Top-down control of phytoplankton biomass and community structure in the monsoonal Arabian Sea. *Limnol. Oceanogr.*, **47**, 1307–1323.

Goericke, R. and Montoya, J. (1998) Estimating the contribution of microalgal taxa to chlorophyll *a* in the field—variations of pigment ratios under nutrient- and light-limited growth. *Mar. Ecol. Prog. Ser.*, **169**, 97–112.

Goes, J. E., Gomes, H. D. R., Selph, K. E. and Landry, M. R. (2016) Biological response of Costa Rica Dome phytoplankton to light, silicic acid and trace metals. *J. Plankton Res.*, **38**, 290–304.

Gordon, L. I., Jennings, J. C., Ross, A. A. and Krest, J. M. (1992) A suggested protocol for continuous flow automated analysis of seawater nutrients in the WOCE hydrographic program and the Joint Global Ocean Fluxes Study. Grp. Tech Rpt 92-1, OSU College of Oceanography Descr. Chem Oc.

Jacobson, D. M. and Anderson, D. M. (1996) Widespread phagocytosis of ciliates and other protists by marine mixotrophic and heterotrophic thecate dinoflagellates. *J. Phycol.*, **32**, 279–285.

Jeffrey, S. W. and Wright, S. W. (2005) Photosynthetic pigments in marine microalgae. In Subba Rao, D. V. (ed.), *Algal Cultures, Analogues of Blooms and Applications*. Science Publishers, New Hampshire, pp. 33–90.

Krause, J. W., Stukel, M. R., Taylor, A. G., Taniguchi, D. A., De Verneil, A. and Landry, M. R. (2016) Net biogenic silica production and the contribution of diatoms to new production and organic matter export in the Costa Rica Dome ecosystem. *J. Plankton Res.*, **38**, 216–229.

Landry, M. R., Brown, S. L., Neveux, J., Dupouy, C., Blanchot, J., Christensen, S. and Bidigare, R. R. (2003) Phytoplankton growth and microzooplankton grazing in high-nutrient, low-chlorophyll waters of the equatorial Pacific: community and taxon-specific rate assessments from pigment and flow cytometric analyses. *J. Geophys. Res.*, **108**, 8142. doi:10.1029/200JC00744.

Landry, M. R. and Kirchman, D. L. (2002) Microbial community structure and variability in the tropical Pacific. *Deep-Sea Res. II*, **49**, 2669–2694.

Landry, M. R., Ohman, M. D., Goericke, R., Stukel, M. R. and Tsyrkevich, K. (2009) Lagrangian studies of phytoplankton growth and grazing relationships in a coastal upwelling ecosystem off Southern California. *Prog Oceanogr.*, **83**, 208–126.

Landry, M. R., Ondrusek, M. E., Tanner, S. J., Brown, S. L., Constantinou, J., Bidigare, R. R., Coale, K. H. and Fitzwater, S. (2000) Biological response to iron fertilization in the eastern equatorial Pacific (IronEx II). I. Microplankton community abundances and biomass. *Mar. Ecol. Prog. Ser.*, **201**, 27–42.

Landry, M. R., de Verneil, A., Goes, J. I. and Moffett, J. W. (2016a) Plankton dynamics and biogeochemical fluxes in the Costa Rica Dome: introduction to the CRD flux and zinc experiments. *J. Plankton Res.*, **38**, 167–182.

Landry, M. R., Selph, K. E., Decima, M., Gutiérrez-Rodríguez, A., Stukel, M. R., Taylor, A. G. and Pasulka, A. (2016b) Phytoplankton production and grazing balances in the Costa Rica Dome. *J. Plankton Res.*, **38**, 366–379.

Landry, M. R., Selph, K. E., Taylor, A. G., Décima, M., Balch, W. M. and Bidigare, R. R. (2011) Phytoplankton growth, grazing and production balances in the HNLC equatorial Pacific. *Deep-Sea Res. II*, **58**, 524–535.

Li, W. K. W., Subba Rao, D. V., Harrison, W. G., Smith, J. C., Cullen, J. J., Irwin, B. and Platt, T. (1983) Autotrophic picoplankton in the tropical ocean. *Science*, **219**, 292–295.

Linacre, L., Landry, M. R., Cajal-Medrano, R., Lara-Lara, J. R., Hernández-Ayón, J. M., Mouriño-Pérez, R. R., García-Mendoza, E. and Bazán-Guzmán, C. (2012) Temporal dynamics of carbon flow through the microbial plankton community in a coastal upwelling system off northern Baja California, Mexico. *Mar. Ecol. Prog. Ser.*, **461**, 31–46.

Linacre, L., Landry, M. R., Lara-Lara, J. R., Hernández-Ayón, J. M. and Bazán-Guzmán, C. (2010) Picoplankton dynamics during contrasting seasonal oceanographic conditions at a coastal upwelling station off northern Baja California, Mexico. *J. Plankton Res.*, **32**, 539–557.

McClain, C. R., Christian, J. R., Signorini, S. R., Lewis, M. R., Asanuma, I., Turk, D. and Dupont-Douchement, C. (2002) Satellite ocean-color observations of the tropical Pacific ocean. *Deep-Sea Res. II*, **49**, 2533–2560.

Menden-Deuer, S. and Lessard, E. J. (2000) Carbon to volume relationships for dinoflagellates, diatoms and other protist plankton. *Limnol. Oceanogr.*, **45**, 569–579.

Monger, B. C. and Landry, M. R. (1993) Flow cytometric analysis of marine bacteria with Hoechst 33342. *Appl. Environ. Microbiol.*, **59**, 905–911.

Mouw, C. B. and Yoder, J. A. (2005) Primary production calculations in the Mid-Atlantic Bight including effects of phytoplankton community size structure. *Limnol. Oceanogr.*, **50**, 1232–1243.

Murray, J. W., Barber, R. T., Roman, M. R., Bacon, M. P. and Feely, R. A. (1994) Physical and biological controls on carbon cycling in the equatorial Pacific. *Science*, **266**, 58–65.

Nelson, D. M. and Landry, M. R. (2011) Regulation of phytoplankton production and upper-ocean biogeochemistry in the eastern equatorial Pacific: introduction to results of the Equatorial Biocomplexity project. *Deep-Sea Res. II*, **58**, 277–283.

Pasulka, A. L., Landry, M. R., Taniguchi, D. A. A., Taylor, A. G. and Church, M. J. (2013) Temporal dynamics of phytoplankton and heterotrophic protists at station ALOHA. *Deep-Sea Res.*, **93**, 44–57.

Reilly, S. B. and Thayer, V. G. (1990) Blue whale (*Balaenoptera musculus*) distribution in the eastern tropical Pacific. *Mar. Mammal Sci.*, **6**, 265–277.

Saito, M. A., Rocap, G. and Moffett, J. W. (2005) Production of cobalt binding ligands in a Synechococcus feature at the Costa Rica upwelling dome. *Limnol. Oceanogr.*, **50**, 279–290.

Sanders, R. W. (1991) Mixotrophic protists in marine and freshwater ecosystems. *J. Protozool.*, **38**, 76–81.

Sameoto, D. D. (1986) Influence of the biological and physical environment on the vertical distribution of mesozooplankton and micronekton in the eastern tropical Pacific. *Mar. Biol.*, **93**, 263–279.

Selph, K. E., Landry, M. R., Taylor, A. G., Gutiérrez-Rodríguez, A., Stukel, M. R., Wokuluk, J. and Pasulka, A. (2016) Phytoplankton production and taxon-specific growth rates in the Costa Rica Dome. *J. Plankton Res.*, **38**, 199–215.

Selph, K. E., Landry, M. R., Taylor, A. G., Yang, E. J., Measures, C. I., Yang, J. J., Stukel, M. R., Christensen, S. *et al.* (2011) Spatially-resolved, taxon-specific phytoplankton production and grazing dynamics in relation to iron distributions in the Equatorial Pacific between 110 and 140°W. *Deep-Sea Res. II*, **58**, 358–377.

Sherr, E. B. and Sherr, B. F. (1993) Preservation and storage of samples for enumeration of heterotrophic protists. In Kemp, P. K. (ed.), *Handbook of Methods in Aquatic Microbial Ecology*. CRC Press, Boca Raton, FL, pp. 207–212.

Stoecker, D. K. (1999) Mixotrophy among dinoflagellates. *J. Eukaryot. Microbiol.*, **46**, 397–401.

Tangen, K. and Björnland, T. (1981) Observations on pigments and morphology of *Gyrodinium aureolum* Hulburt, a marine dinoflagellate containing 19′-hexanoyloxyfucoxanthin as the main carotenoid. *J. Plankton Res.*, **3**, 389–401.

Taylor, A. G., Landry, M. R., Selph, K. E. and Yang, E. J. (2011) Biomass, size structure and depth distributions of the microbial community in the eastern equatorial Pacific. *Deep-Sea Res. II*, **58**, 342–357.

Taylor, A. G., Landry, M. R., Selph, K. E. and Wokuluk, J. J. (2014) Temporal and spatial patterns of microbial community biomass and composition in the Southern California Current Ecosystem. *Deep-Sea Res. II*, **112**, 117–128.

Vecchione, M. (1999) Extraordinary abundance of squid paralarve in the tropical eastern Pacific ocean during El Nino of 1987. *Fish. Bull.*, **97**, 1025–1030.

Vilchis, L. I., Ballance, L. T. and Fiedler, P. C. (2006) Pelagic habitat of seabirds in the eastern tropical Pacific: effects of foraging ecology on habitat selection. *Mar. Ecol. Prog. Ser.*, **315**, 279–292.

Wyrtki, K. (1964) Upwelling in the Costa Rica Dome. *Fish. Bull.*, **63**, 355–372.

Zar, J. H. (1984) *Biostatistical Analysis*, 2nd edn. Prentice-Hall, Inc., Englewood Cliffs, NJ. 718 p.